

# Create a polarization insensitive lens by quasiisotropic metamaterial slab

Hailu Luo,\* Zhongzhou Ren, Weixing Shu, and Fei Li

*Department of Physics, Nanjing University, Nanjing 210008, China*

(Dated: February 9, 2020)

## Abstract

We propose to employ the quasiisotropic metamaterial (QIMM) slab to create a polarization insensitive lens, in which both E- and H-polarized waves exhibit the same refocusing effect. For shallow incident angles, the QIMM slab will provide some degree of refocusing in the same manner as an isotropic negative index material. The refocusing effect allows us to introduce the ideas of paraxial beam focusing and phase compensation by the QIMM slab. On the basis of angular spectrum representation, a formalism describing paraxial beams propagating through a QIMM slab is presented. Because of the negative phase velocity in the QIMM slab, the inverse Gouy phase shift and the negative Rayleigh length of paraxial Gaussian beam are proposed. We found that the phase difference caused by the Gouy phase shift in vacuum can be compensated by that caused by the inverse Gouy phase shift in the QIMM slab. If certain matching conditions are satisfied, the intensity and phase distributions at object plane can be completely reconstructed at the image plane.

PACS numbers: 78.20.Ci, 41.20.Jb, 42.25.Gy

Keywords: polarization insensitive lens, quasiisotropic metamaterial, negative refraction

---

\*Author to whom correspondence should be addressed. E-mail: hailuluo@sohu.com

## I. INTRODUCTION

About forty years ago, Veselago firstly introduced the concept of left-handed material (LHM) in which both the permittivity  $\epsilon$  and the permeability  $\mu$  are negative [1]. He predicted that LHM would have unique and potentially interesting properties, such as the negative refraction index, the reversed Doppler shift and the backward Cerenkov radiation. Veselago pointed out that electromagnetic waves incident on a planar interface between a regular material and a LHM will undergo negative refraction. Hence a LHM planar slab can act as a lens and focus waves from a point source. LHM did not receive much attention as it only existed in a conceptual form. After the first experimental observation of negative refraction using a metamaterial composed of split ring resonators (SRR) [2, 3], the study of such materials has received increasing attention over the last few years. While negative refraction is most easily visualized in an isotropic metamaterial [2, 3, 4, 5, 6], negative refraction can also be realized in photonic crystals [7, 8, 9, 10] and anisotropic metamaterials [11, 12, 13, 14, 15, 16] have also been reported.

Recently, Pendry extended Veselago's analysis and further predicted that a LHM slab can amplify evanescent waves and thus behaves like a perfect lens [17]. He proposed that the amplitudes of evanescent waves from a near-field object could be restored at its image. Therefore, the spatial resolution of the superlens can overcome the diffraction limit of conventional imaging systems and reach the subwavelength scale. The great research interests were initiated by the revolutionary concept. More recently, the anisotropic metamaterials have proved to be good candidates for slab lens application [18, 19, 20, 21]. Although the focusing is imperfect, the substantial field intensity enhancement can readily be observed. In these cases, the anisotropic metamaterials under consideration are characterized by a hyperboloid wave-vector surface, and the focusing is restricted to either E- or H-polarized radiation. The recent development in quasiisotropic metamaterial (QIMM) offer further opportunities to extend the previous work and further predict that both E- and H-polarized waves can be refocused.

The main purpose of the present work is to construct a polarization insensitive lens by a QIMM slab. For shallow incident angles the QIMM slab will provide some degree of refocusing in the same manner as an isotropic negative index material. We show that both E- and H-polarized waves can exhibit the same refocusing effect. Starting from the representation of plane-wave angular spectrum, we derive the propagation of paraxial beams

in the QIMM slab. Our formalism permits us to introduce ideas for beam focusing and phase compensation of paraxial beams by using the QIMM slab. Because of the negative anisotropic parameters, the inverse Gouy phase shift and negative Rayleigh length in the QIMM slab are proposed. As an example, we obtain the analytical description for a Gaussian beam propagating through a QIMM slab. We find that the phase difference caused by the Gouy phase shift in isotropic RHM can be compensated by that caused by the inverse Gouy phase shift in the QIMM slab. If certain matching conditions are satisfied, the intensity and phase distributions at object plane can be completely reconstructed at the image plane.

## II. POLARIZATION INSENSITIVE METAMATERIAL

Before we consider the polarization insensitive lens, we first analyze what is the QIMM. For anisotropic materials, one or both of the permittivity and permeability are second-rank tensors. In the following we assume that both the permittivity and permeability tensors are simultaneously diagonalizable:

$$\boldsymbol{\epsilon} = \begin{pmatrix} \epsilon_x & 0 & 0 \\ 0 & \epsilon_y & 0 \\ 0 & 0 & \epsilon_z \end{pmatrix}, \quad \boldsymbol{\mu} = \begin{pmatrix} \mu_x & 0 & 0 \\ 0 & \mu_y & 0 \\ 0 & 0 & \mu_z \end{pmatrix}. \quad (1)$$

where  $\epsilon_i$  and  $\mu_i$  ( $i = x, y, z$ ) are the permittivity and permeability constants in the principal coordinate system.

Following the standard procedure, we consider a monochromatic electromagnetic field  $\mathbf{E}(\mathbf{r}, t) = \text{Re}[\mathbf{E}(\mathbf{r}) \exp(-i\omega t)]$  and  $\mathbf{B}(\mathbf{r}, t) = \text{Re}[\mathbf{B}(\mathbf{r}) \exp(-i\omega t)]$  of angular frequency  $\omega$  incident from vacuum into the anisotropic metamaterial. The field can be described by Maxwell's equations [22]

$$\begin{aligned} \nabla \times \mathbf{E} &= -\frac{\partial \mathbf{B}}{\partial t}, & \mathbf{B} &= \mu_0 \boldsymbol{\mu} \cdot \mathbf{H}, \\ \nabla \times \mathbf{H} &= \frac{\partial \mathbf{D}}{\partial t}, & \mathbf{D} &= \epsilon_0 \boldsymbol{\epsilon} \cdot \mathbf{E}. \end{aligned} \quad (2)$$

The previous Maxwell equations can be combined in a straightforward way to obtain the well-known equation for the complex amplitude of the electric field in the anisotropic metamaterial, and reads as

$$\nabla \times (\boldsymbol{\mu}^{-1} \cdot \nabla \times \mathbf{E}) + \frac{1}{c^2} \frac{\partial^2 \mathbf{D}}{\partial t^2} = 0, \quad (3)$$

where  $c$  is the speed of light in the vacuum.

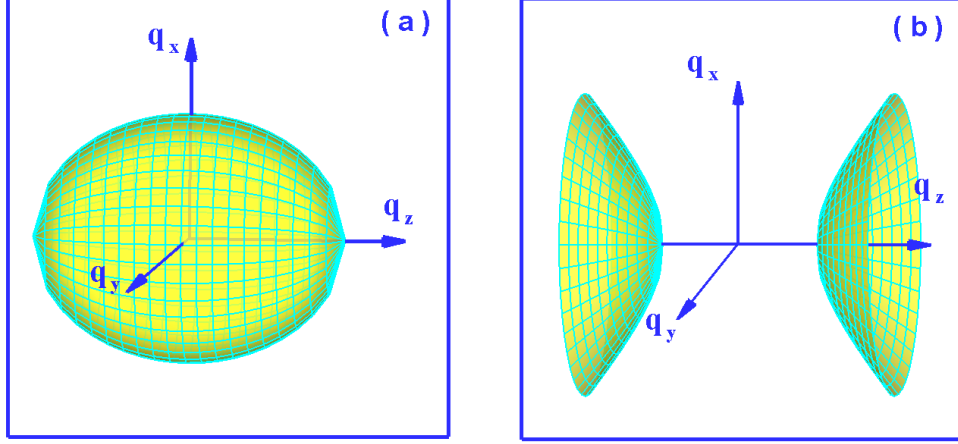


FIG. 1: (a) The quasiisotropic metamaterial with ellipsoid wave-vector surface, (b) The quasi-isotropic metamaterial with single-sheeted wave-vector surface.

In the principal coordinate system, Maxwell's equations yield a scalar wave equation. In free space, the accompanying dispersion relation has the familiar form

$$k_x^2 + k_y^2 + k_z^2 = \frac{\omega^2}{c^2}, \quad (4)$$

where  $k_i$  is the  $i$  component of the incident wave vector.

Because of the importance in achieving the polarization insensitive effect, we will focus our interesting in the anisotropic metamaterial, in which the permittivity and permeability tensor elements satisfy the condition:

$$\frac{\varepsilon_x}{\mu_x} = \frac{\varepsilon_y}{\mu_y} = \frac{\varepsilon_z}{\mu_z} = C \quad (C > 0), \quad (5)$$

where  $C$  is a constant. A careful calculation of the Maxwell equations gives the dispersion relation:

$$\left( \frac{q_x^2}{\varepsilon_z \mu_y} + \frac{q_y^2}{\varepsilon_z \mu_x} + \frac{q_z^2}{\varepsilon_y \mu_x} - \frac{\omega^2}{c^2} \right) \left( \frac{q_x^2}{\varepsilon_y \mu_z} + \frac{q_y^2}{\varepsilon_x \mu_z} + \frac{q_z^2}{\varepsilon_x \mu_y} - \frac{\omega^2}{c^2} \right) = 0, \quad (6)$$

where  $q_i$  represents the  $i$  component of transmitted wave-vector. The above equation can be represented by a three-dimensional surface in wave-vector space. This surface is known as the normal surface and consists of two shells. Under the condition of Eq. (5), we can find E- and H-polarized waves have the same wave-vector surface. Thus the anisotropic medium also be regard as QIMM [23, 24]. Clearly, we can find the dispersion surface has following two types: ellipsoid, single-sheeted hyperboloid and double-sheeted hyperboloid, as show in Fig. 1

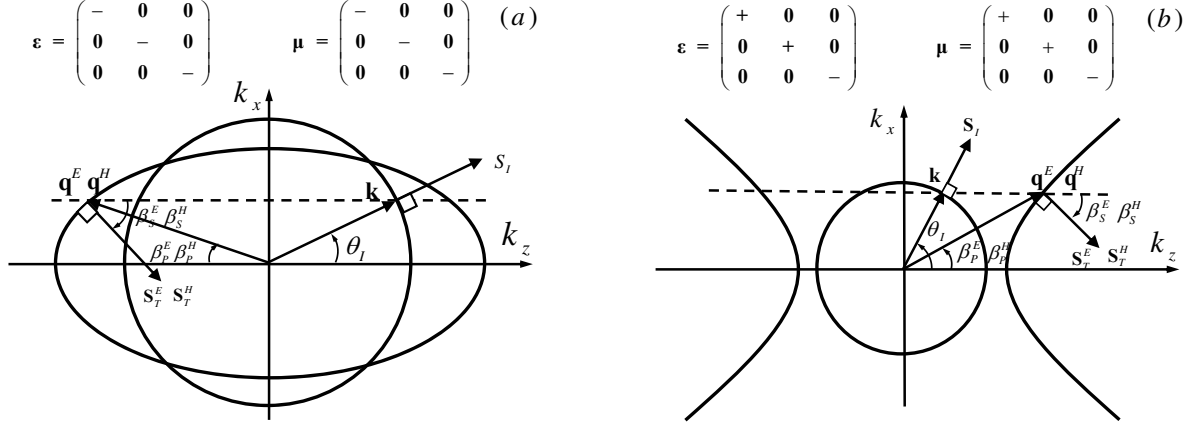


FIG. 2: The circle and hyperbola represent the dispersion relations of isotropic and quasiisotropic media, respectively. The incident wave vector  $\mathbf{k}$  is parallel to the Poynting vector  $\mathbf{S}_I$  in vacuum. Because of the anisotropy in QIMM,  $\mathbf{S}_T$  must lie normal to the frequency contour. The wave vector undergoes a negative refraction, while the energy flow undergoes positive refraction.

Now, a question is easily answered whether E- and H-polarized exhibit the same propagation character. We choose the  $z$  axis to be normal to the interface, the  $x$  and  $y$  axes locate at in the plane of the interface. The  $z$ -component of the wave vector can be found by the solution of Eq. (6), which yields

$$q_z^E = \sigma \sqrt{\epsilon_y \mu_x k_0^2 - \epsilon_y \mu_x \left( \frac{q_x^2}{\epsilon_z \mu_y} + \frac{q_y^2}{\epsilon_z \mu_x} \right)}, \quad (7)$$

$$q_z^H = \sigma \sqrt{\epsilon_x \mu_y k_0^2 - \epsilon_x \mu_y \left( \frac{q_x^2}{\epsilon_y \mu_z} + \frac{q_y^2}{\epsilon_x \mu_z} \right)}, \quad (8)$$

for E- and H-polarized waves, respectively. Here  $k_0 = \omega/c$  is the wave number in vacuum and  $\sigma = \pm 1$ . This choice of sign ensures that power propagates away from the boundary to the  $+z$  direction.

Without loss of generality, we assume the wave vector locate in the  $x - z$  plane ( $k_y = q_y = 0$ ). The incident angle of light is given by

$$\theta_I = \tan^{-1} \left[ \frac{k_x}{k_z} \right]. \quad (9)$$

The values of refractive wave vector can be found by using the boundary conditions and dispersion relations. The refractive angle of the transmitted wave vector or phase of E- and

H- polarized waves can be written as

$$\beta_P^E = \tan^{-1} \left[ \frac{q_x^E}{q_z^E} \right], \quad \beta_P^H = \tan^{-1} \left[ \frac{q_x^H}{q_z^H} \right]. \quad (10)$$

After the dispersion relation and the refraction angle are determined, we will discuss the reflection and transmission coefficients in the following section. It should be noted the actual direction of light is defined by the time-averaged Poynting vector  $\mathbf{S} = \frac{1}{2} \mathbf{Re}(\mathbf{E}^* \times \mathbf{H})$ . For E- and H-polarized refracted waves,  $\mathbf{S}_T$  is given by

$$\mathbf{S}_T^E = \text{Re} \left[ \frac{T_E^2 E_0^2 q_x^E}{2\omega\mu_z} \mathbf{e}_x + \frac{T_E^2 E_0^2 q_z^E}{2\omega\mu_x} \mathbf{e}_z \right], \quad (11)$$

$$\mathbf{S}_T^H = \text{Re} \left[ \frac{T_H^2 E_0^2 q_x^H}{2\omega\varepsilon_z} \mathbf{e}_x + \frac{T_H^2 E_0^2 q_z^H}{2\omega\varepsilon_x} \mathbf{e}_z \right], \quad (12)$$

There is a bending angle between  $\mathbf{q}$  and  $\mathbf{S}$ , and therefore  $\mathbf{q}$ ,  $\mathbf{E}$  and  $\mathbf{H}$  do not form a strictly left-handed system in QIMM. The refraction angle of Poynting vector of E- and H- polarized incident waves can be obtained as

$$\beta_S^E = \tan^{-1} \left[ \frac{S_{Tx}^E}{S_{Tz}^E} \right], \quad \beta_S^H = \tan^{-1} \left[ \frac{S_{Tx}^H}{S_{Tz}^H} \right]. \quad (13)$$

Combining Eq. (10) and (13) we can easily find that E- and H- polarized waves have the same refraction properties.

Now we are in the position to study the negative refraction in the QIMM. Unlike in isotropic media, the Poynting vector in The QIMM is neither parallel nor antiparallel to the wave vector, but rather makes either an acute or an obtuse angle with respect to the wave vector. In general, to distinguish the positive and negative refraction in quasiisotropic media, we must calculate the direction of the Poynting vector with respect to the wave vector. Positive refraction means  $\mathbf{q}_x \cdot \mathbf{S}_T > 0$ , and negative refraction means  $\mathbf{q}_x \cdot \mathbf{S}_T < 0$  [24]. From Eqs. (11) and (12) we get

$$\mathbf{q}_x \cdot \mathbf{S}_T^E = \frac{T_E^2 E_0^2 q_x^2}{2\omega\mu_z}, \quad \mathbf{q}_x \cdot \mathbf{S}_T^H = \frac{T_H^2 H_0^2 q_x^2}{2\omega\varepsilon_z}. \quad (14)$$

The negative refraction phenomenon is one of the most interesting peculiar properties of the QIMM. We can see that the refracted waves will be determined by  $\mu_z$  for E-polarized incident waves and  $\varepsilon_z$  for H-polarized incident waves.

Because of the importance of refocusing effect, we are intersted the two types of QIMM, which can formed from the combinations of material parameter tensor elements.

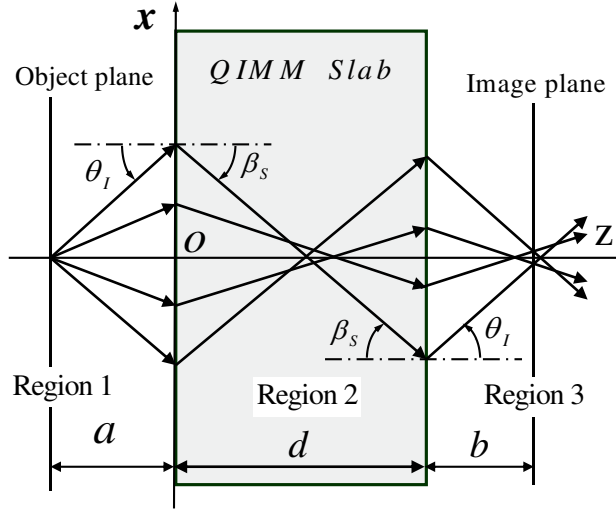


FIG. 3: The ray tracing picture showing the focussing by QIMM slab. The QIMM slab is surrounded by vacuum in region 1 and region 2. The solid line and dash-dotted lines are the theoretical objective and focusing planes respectively.

Type I. In this case all of the  $\varepsilon_i$  and  $\mu_i$  are negative. The frequency contour is the ellipse as shown in Fig. 2a. Here  $\mathbf{k}_z \cdot \mathbf{q}_z < 0$  and  $\mathbf{q}_x \cdot \mathbf{S}_T < 0$ , so the refraction angle of wave vector and Poynting vector are always negative.

Type II. In this case  $\varepsilon_x > 0$ ,  $\varepsilon_y > 0$  and  $\varepsilon_z < 0$ . The wave-vector surface is the single-sheeted hyperbola as depicted in Fig. 2b. Here  $\mathbf{k}_z \cdot \mathbf{q}_z > 0$  and  $\mathbf{q}_x \cdot \mathbf{S}_T < 0$ . It yields that the refraction of Poynting vector refraction is always negative even if the wave-vector refraction is always positive.

As noted above, the Poynting vector will exhibit the negative refraction in the two types of QIMM. The negative refraction is the important effect responsible for the slab lens. To simplify the proceeding analyses, we will focus our attention on the QIMM with ellipsoid wave-vector surface.

### III. THE PARAXIAL MODEL OF BEAM PROPAGATION

In this section, Let us examine the polarization insensitive effect in paraxial regime. As depicted in Fig. 3, the QIMM slab in region 2 is surrounded by vacuum in region 1 and region 3. From the ray tracing picture of Fig. 3, we can easily find that there is a strong astigmatism effect in the image plane.

From a mathematical point of view, the approximate paraxial expression for the field can be obtained by the expansion of the square root of  $q_z$  to the first order in  $|\mathbf{q}_\perp|/q$  [26, 27, 28], which yields

$$q_z^E = \sigma \sqrt{\varepsilon_y \mu_x} k_0 + \left( \frac{\sigma \sqrt{\varepsilon_y \mu_x} k_x^2}{2\varepsilon_z \mu_y k_0} + \frac{\sigma \sqrt{\varepsilon_y \mu_x} k_y^2}{2\varepsilon_z \mu_x k_0} \right), \quad (15)$$

$$q_z^H = \sigma \sqrt{\varepsilon_x \mu_y} k_0 + \left( \frac{\sigma \sqrt{\varepsilon_x \mu_y} k_x^2}{2\varepsilon_y \mu_z k_0} + \frac{\sigma \sqrt{\varepsilon_x \mu_y} k_y^2}{2\varepsilon_x \mu_z k_0} \right), \quad (16)$$

For shallow incident angles the QIMM slab will provide some degree of refocusing in the same manner as an isotropic negative index material, as shown in Fig. 4. Hence the interesting property allow us introduce the idea to construct a anisotropic matamaterial slab lens in paraxial beam region.

Equation (3) can be conveniently solved by employing the Fourier transformations, so the complex amplitude in RHM and LHM can be conveniently expressed as

$$\mathbf{E}(\mathbf{r}_\perp, z) = \int d^2 \mathbf{k}_\perp \tilde{E}(\mathbf{k}_\perp) \exp[i\mathbf{k}_\perp \cdot \mathbf{r}_\perp + iq_z z]. \quad (17)$$

Here  $\mathbf{r}_\perp = x\mathbf{e}_x + y\mathbf{e}_y$ ,  $\mathbf{k}_\perp = k_x\mathbf{e}_x + k_y\mathbf{e}_y$ , and  $\mathbf{e}_j$  is the unit vector in the  $j$ -direction.

Eqs. (15) and (15) into Eq. (17), respectively, we obtain

$$\begin{aligned} \mathbf{E}_E(\mathbf{r}_\perp, z) = & \exp(i\sigma \sqrt{\varepsilon_y \mu_x} k_0 z) \int d^2 \mathbf{k}_\perp \\ & \times \exp \left[ i\mathbf{k}_\perp \cdot \mathbf{r}_\perp - \left( \frac{\sigma \sqrt{\varepsilon_x \mu_y}}{2\varepsilon_y \mu_z k_0} k_x^2 + \frac{\sigma \sqrt{\varepsilon_x \mu_y}}{2\varepsilon_x \mu_z k_0} k_y^2 \right) \right] \tilde{\mathbf{E}}(\mathbf{k}_\perp). \end{aligned} \quad (18)$$

$$\begin{aligned} \mathbf{E}_H(\mathbf{r}_\perp, z) = & \exp(i\sigma \sqrt{\varepsilon_x \mu_y} k_0 z) \int d^2 \mathbf{k}_\perp \\ & \times \exp \left[ i\mathbf{k}_\perp \cdot \mathbf{r}_\perp - \left( \frac{\sigma \sqrt{\varepsilon_y \mu_x}}{2\varepsilon_z \mu_y k_0} k_x^2 + \frac{\sigma \sqrt{\varepsilon_y \mu_x}}{2\varepsilon_z \mu_x k_0} k_y^2 \right) \right] \tilde{\mathbf{E}}(\mathbf{k}_\perp). \end{aligned} \quad (19)$$

The field  $\tilde{E}(\mathbf{k}_\perp)$  In Eqs. (18) and (19) are related to the boundary distribution of the electric field by means of the relation

$$\tilde{\mathbf{E}}_E(\mathbf{k}_\perp) = \int d^2 \mathbf{r}_\perp \mathbf{E}_E(\mathbf{r}_\perp, 0) \exp[i\mathbf{k}_\perp \cdot \mathbf{r}_\perp], \quad (20)$$

$$\tilde{\mathbf{E}}_H(\mathbf{k}_\perp) = \int d^2 \mathbf{r}_\perp \mathbf{E}_H(\mathbf{r}_\perp, 0) \exp[i\mathbf{k}_\perp \cdot \mathbf{r}_\perp], \quad (21)$$

for E- and H-polarized waves, respectively. Evidently, Eqs. (20) and (21) are standard two-dimensional Fourier transform [25]. In fact, after the electric field on the plane  $z = 0$  is



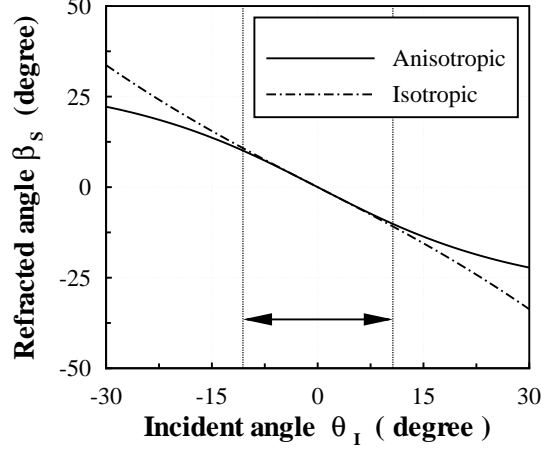


FIG. 4: For shallow incident angles, the QIMM slab will provide some degree of refocusing in the same manner as an isotropic negative index material.

known, Eqs. (18) and (19) provide the expression of the E- and H-polarized field in the space  $z > 0$ , respectively.

Since our attention will be focused on beam propagating along the  $+z$  direction, we can write the paraxial fields as

$$\mathbf{E}_E(\mathbf{r}_\perp, z) = \mathbf{A}_E(\mathbf{r}_\perp, z) \exp(i\sigma\sqrt{\varepsilon_y\mu_x}k_0z), \quad (22)$$

$$\mathbf{E}_H(\mathbf{r}_\perp, z) = \mathbf{A}_H(\mathbf{r}_\perp, z) \exp(i\sigma\sqrt{\varepsilon_x\mu_y}k_0z), \quad (23)$$

where the field  $A(\mathbf{r}_\perp, z)$  is the slowly varying envelope amplitude which satisfies the parabolic equation

$$\left[ i\frac{\partial}{\partial z} + \left( \frac{\sigma\sqrt{\varepsilon_x\mu_y}}{2\varepsilon_y\mu_zk_0} \frac{\partial^2}{\partial x^2} + \frac{\sigma\sqrt{\varepsilon_x\mu_y}}{2\varepsilon_x\mu_zk_0} \frac{\partial^2}{\partial y^2} \right) \right] \mathbf{A}_E(\mathbf{r}_\perp, z) = 0, \quad (24)$$

$$\left[ i\frac{\partial}{\partial z} + \left( \frac{\sigma\sqrt{\varepsilon_y\mu_x}}{2\varepsilon_z\mu_yk_0} \frac{\partial^2}{\partial x^2} + \frac{\sigma\sqrt{\varepsilon_y\mu_x}}{2\varepsilon_z\mu_xk_0} \frac{\partial^2}{\partial y^2} \right) \right] \mathbf{A}_H(\mathbf{r}_\perp, z) = 0, \quad (25)$$

Under the quasiisotropic condition of Eq. (5), we can easily find that E- and H-polarized paraxial field exhibit the same propagating characteristics in paraxial regime. The interesting properties allow us introduce the idea to construct a polarization lens by QIMM slab. For simplify, we introduce the effective refraction indexes:

$$n_x = \sigma \frac{\varepsilon_y\mu_z}{\sqrt{\varepsilon_x\mu_y}}, \quad n_y = \sigma \frac{\varepsilon_x\mu_z}{\sqrt{\varepsilon_x\mu_y}}. \quad (26)$$

From Eqs. (24) and (25) we can find that the field of paraxial beams in QIMM can be written in the similar way to that in regular material, while the sign of the effective refraction index is reverse.

#### IV. BEAM FOCUSING BY POLARIZATION INSENSITIVE LENS

The previous section we have understand both E- and H-polarized beams have the same propagation character in QIMM slab. Hence we do not wish involve in the trouble to discuss the focusing effect of two polarized waves. In this section we will investigate the analytical description for E-polarized beam with a boundary Gaussian distribution. This example allows us to describe the refocusing features of beam propagation in QIMM slab. The beam will pass the interfaces  $z = a$  and  $z = a + d$  before it reaches the image plane  $z = a + b + d$ . To be uniform throughout the following analysis, we introduce different coordinate transformations  $z_i^* (i = 1, 2, 3)$  in the three regions, respectively. First we want to explore the field in region 1. Without any loss of generality, we assume that the input waist locates at the object plane  $z = 0$ . The fundamental Gaussian spectrum distribution can be written in the form

$$\tilde{\mathbf{E}}_1(\mathbf{k}_\perp) = \frac{w_0 E_0}{\sqrt{2\pi}} \exp \left[ -\frac{k_\perp^2 w_0^2}{4} \right], \quad (27)$$

where  $w_0$  is the spot size. By substituting Eq. (27) into Eq. (17), the field in the region 1 can be written as

$$\mathbf{E}_1(\mathbf{r}_\perp, z_1^*) = \frac{w_0 E_0}{\sqrt{w_{1x} w_{1y}}} \exp \left[ -\left( \frac{x^2}{w_{1x}^2} + \frac{y^2}{w_{1y}^2} \right) + i\psi_1 \right], \quad (28)$$

$$w_{1x} = w_0 \sqrt{1 + \left( \frac{z_{1x}^*}{L_{1x}} \right)^2}, \quad w_{1y} = w_0 \sqrt{1 + \left( \frac{z_{1y}^*}{L_{1y}} \right)^2}. \quad (29)$$

Here we have chosen different waists,  $w_{1x}$  and  $w_{1y}$ , in order to deal with a more general situation. Because of the isotropy in vacuum, we can easily obtain  $z_{1x}^* = z_{1y}^* = z$  and  $w_{1x} = w_{1y}$ . The corresponding Rayleigh lengths give by  $L_{1x} = L_{1y} = k_0 w_0^2/2$ .

We are now in a position to investigate the field in region 2. In fact, the field in the first boundary can be easily obtained from Eq. (28) by choosing  $z = a$ . Substituting the field into Eq. (20), the angular spectrum distribution can be obtained as

$$\tilde{\mathbf{E}}_2(\mathbf{k}_\perp) = \frac{w_0 E_0}{\sqrt{2\pi}} \exp \left[ -\frac{k_0 w_0^2 + 2ia}{4k_0} (k_x^2 + k_y^2) \right], \quad (30)$$

For simplicity, we assume that the wave propagates through the boundary without reflection. Substituting Eq. (30) into Eq. (18), the field in the QIMM slab can be written as

$$\mathbf{E}_2(\mathbf{r}_\perp, z_2^*) = \frac{w_0 E_0}{\sqrt{w_{2x} w_{2y}}} \exp \left[ - \left( \frac{x^2}{w_{2x}^2} + \frac{y^2}{w_{2y}^2} \right) + i\psi_2 \right], \quad (31)$$

$$w_{2x} = w_0 \sqrt{1 + \left( \frac{z_{2x}^*}{L_{2x}} \right)^2}, \quad w_{2y} = w_0 \sqrt{1 + \left( \frac{z_{2y}^*}{L_{2y}} \right)^2}. \quad (32)$$

Here  $z_{2x}^* = z - (1 - n_x)a$  and  $z_{2y}^* = z - (1 - n_y)a$ . The interesting point we want to stress is that there are two different Rayleigh lengths,  $L_{2x} = n_x k_0 w_0^2/2$  and  $L_{2y} = n_y k_0 w_0^2/2$ , that characterize the spreading of the beam in the direction of  $x$  and  $y$  axes, respectively. A further important point should be noted that we have introduced the negative Rayleigh length. The inherent physics underlying the negative Rayleigh length is that the waves undergo a negative phase velocity in the QIMM slab. As we will see in the following, the negative Rayleigh length will give rise to the corresponding reverse Gouy phase shift.

Finally we want to explore the field in region 3. The field in the second boundary can be easily obtained from Eq. (31) under choosing  $z = a + d$ . Substituting the field into Eq. (20), the angular spectrum distribution can be written as

$$\tilde{\mathbf{E}}_3(\mathbf{k}_\perp) = \frac{w_0 E_0}{\sqrt{2\pi}} \exp \left[ - \left( \frac{n_x k_0 w_0^2 + 2in_x a + 2id}{4n_x k_0} k_x^2 + \frac{n_y k_0 w_0^2 + 2in_y a + 2id}{4n_y k_0} k_y^2 \right) \right]. \quad (33)$$

Substituting Eq. (33) into Eq. (18), the field in the region 3 is given by

$$\mathbf{E}_3(\mathbf{r}_\perp, z_3^*) = \frac{w_0 E_0}{\sqrt{w_{3x} w_{3y}}} \exp \left[ - \left( \frac{x^2}{w_{3x}^2} + \frac{y^2}{w_{3y}^2} \right) + i\psi_3 \right], \quad (34)$$

$$w_{3x} = w_0 \sqrt{1 + \left( \frac{z_{3x}^*}{L_{3x}} \right)^2}, \quad w_{3y} = w_0 \sqrt{1 + \left( \frac{z_{3y}^*}{L_{3y}} \right)^2}. \quad (35)$$

Here  $z_{3x}^* = z - (1 - 1/n_x)d$  and  $z_{3y}^* = z - (1 - 1/n_y)d$ . The corresponding Rayleigh lengths give by  $L_{3x} = L_{3y} = k_0 w_0^2/2$ , that denote the beam exhibits the same diffraction distance in the direction of  $x$  and  $y$  axes. The effect of the anisotropic diffraction is that these two beam widths keep their difference even if the Rayleigh lengths,  $L_{3x}$  and  $L_{3y}$ , are equal, implying that generally the Gaussian beam is astigmatic.

Up to now, the fields are determined explicitly in the three regions. Comparing Eq. (31), Eq. (34) with Eq. (28) show that the field distributions in region 2 and region 3 may no

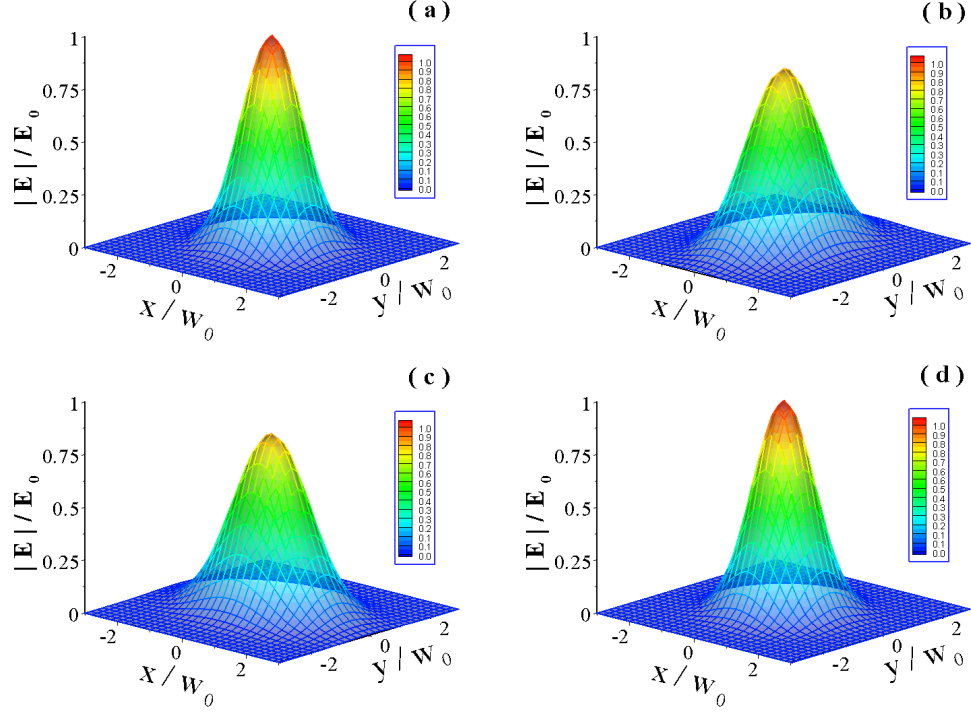


FIG. 5: The numerically computed intensity distribution in object and image planes. (a) the intensity distribution for normal Gaussian beam in object plane. The intensity distribution in image plane for Gaussian beam propagating through the QIMM slab with different anisotropic parameters: (b)  $n_x = -1$ ,  $n_y = -2$ . (c)  $n_x = -2$ ,  $n_y = -1$ . (d)  $n_x = -1$ ,  $n_y = -1$ . We can easily find the intensity distribution at the object plane can be completely reconstructed at the image plane.

longer remain Gaussian. We take the image position  $z = a + d + b$  to be the place of the second focusing waist. For the purpose of illustration, the intensity distribution in object plane is plotted in Fig. 5a. In general, the shape of intensity distribution is distorted in image plane as shown in Fig. 5b and Fig. 5c. Careful evaluation of Eq. (34) reveal that the secret underlying the intensity distortion is the anisotropic diffraction.

Next, the most obvious question is whether the intensity distribution at the object plane can be completely reconstructed at the image plane. In the next step, we want to explore the matching condition of focusing. We can easily obtain the place of the focusing waist by choosing  $z_i^* = 0$ . Let us assume the incident beam waist locates at plane  $z = 0$ . To eliminate the astigmatic effect, the beam waists should locate the same place, namely  $z_{3x}^* = z_{3y}^*$ . Using

these criterions, the matching condition for focusing can be written as

$$\varepsilon_y \mu_z (a + b) + \sigma \sqrt{\varepsilon_x \mu_y} d = 0, \quad \varepsilon_x = \varepsilon_y. \quad (36)$$

Under the focusing matching condition, the intensity distribution at the object plane can be completely reconstructed at the image plane Fig. 5d. A further point should be noted is that the thickness of the QIMM slab should satisfy the relation  $d > \sigma \varepsilon_y \mu_z a / \sqrt{\varepsilon_x \mu_y}$ , otherwise there is neither an internal nor an external focus.

## V. PHASE COMPENSATION BY POLARIZATION INSENSITIVE LENS

In this section, we attempt to investigate the matching condition for phase compensation. In isotropic LHM, plane waves can propagate with negative phase velocity directed opposite to the direction of Poynting vector. Hence the phase difference can be compensated by the LHM slab [1, 17, 24]. However, the negative tensor parameters associated with anisotropic medium provides a wealth of opportunities for observing and exploiting negative phase-velocity behavior.

First let us investigate the phase distribution in region 1. A more rigorous calculation of Eq. (28) give the phase

$$\psi_1 = k_0 z + \left( \frac{k_0 x^2}{2R_{1x}} + \frac{k_0 y^2}{2R_{1y}} \right) - \Phi_1, \quad (37)$$

$$R_{1x} = z_{1x}^* + \frac{L_{1x}^2}{z_{1x}^*}, \quad R_{1y} = z_{1y}^* + \frac{L_{1y}^2}{z_{1y}^*} \quad (38)$$

$$\Phi_1 = -\frac{1}{2} \left( \arctan \frac{z_{1x}^*}{L_{1x}} + \arctan \frac{z_{1y}^*}{L_{1y}} \right) \quad (39)$$

Here  $R_{1x}$  and  $R_{1y}$  are the radius of curvature. Because of the isotropy in vacuum, we can easily find  $R(z_{1x}^*) = R(z_{1y}^*)$ . The Gouy phase shift in vacuum is given by  $\Phi_1$ .

Next, we attempt to explore the phase distribution in region 2. Matching the boundary condition, the phase distribution can be written as

$$\psi_2 = k_0 a + \sigma \sqrt{\varepsilon_y \mu_x} k_0 (z - a) + \frac{k_0 x^2}{2R_{2x}} + \frac{k_0 y^2}{2R_{2y}} - \Phi_2, \quad (40)$$

$$R_{2x} = z_{2x}^* + \frac{L_{2x}^2}{z_{2x}^*}, \quad R_{2y} = z_{2y}^* + \frac{L_{2y}^2}{z_{2y}^*} \quad (41)$$

$$\Phi_2 = -\frac{1}{2} \left( \arctan \frac{z_{2x}^*}{L_{2x}} + \arctan \frac{z_{2y}^*}{L_{2y}} \right). \quad (42)$$

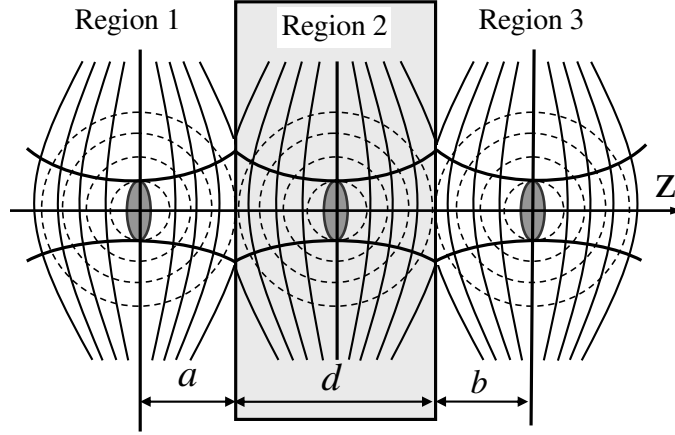


FIG. 6: The phase difference caused by the Gouy phase shift in vacuum can be compensated by that caused by the inverse Gouy phase shift in the QIMM slab. The phase fronts of Gaussian beam (solid lines) differ from those of a perfect spherical wave (dashed lines).

We should mention that there are two different radius of curvature,  $R_{2x}$  and  $R_{2y}$ , that characterize the beam undergo different diffraction effects in the direction of  $x$  and  $y$  axes, respectively.

Now, we are in the position to explore the phase distribution in region 3. Analogously, the phase distribution in region 3 give by

$$\psi_3 = \sigma\sqrt{\varepsilon_y\mu_x}k_0d + k_0(z - d) + \frac{k_0x^2}{2R_{3x}} + \frac{k_0y^2}{2R_{3y}} - \Phi_3, \quad (43)$$

$$R_{3x} = z_{3x}^* + \frac{L_{3x}^2}{z_{3x}^*}, \quad R_{3y} = z_{3y}^* + \frac{L_{3y}^2}{z_{3y}^*}, \quad (44)$$

$$\Phi_3 = -\frac{1}{2} \left( \arctan \frac{z_{3x}^*}{L_{3x}} + \arctan \frac{z_{3y}^*}{L_{3y}} \right). \quad (45)$$

The radius of curvatures are given by Eq. (44). The Gouy phase shift in QIMM is given by Eq. (45). The anisotropic effect result in the two radius of curvatures keep their difference even if the Rayleigh lengths are equal.

It is known that an electromagnetic beam propagating through a focus experiences an additional  $\pi$  phase shift with respect to a plane wave. This phase anomaly was discovered by Gouy in 1890 and has since been referred to as the Gouy phase shift [22, 29]. It should be mentioned that there exists an effect of accumulated Gouy phase shift when a beam passing

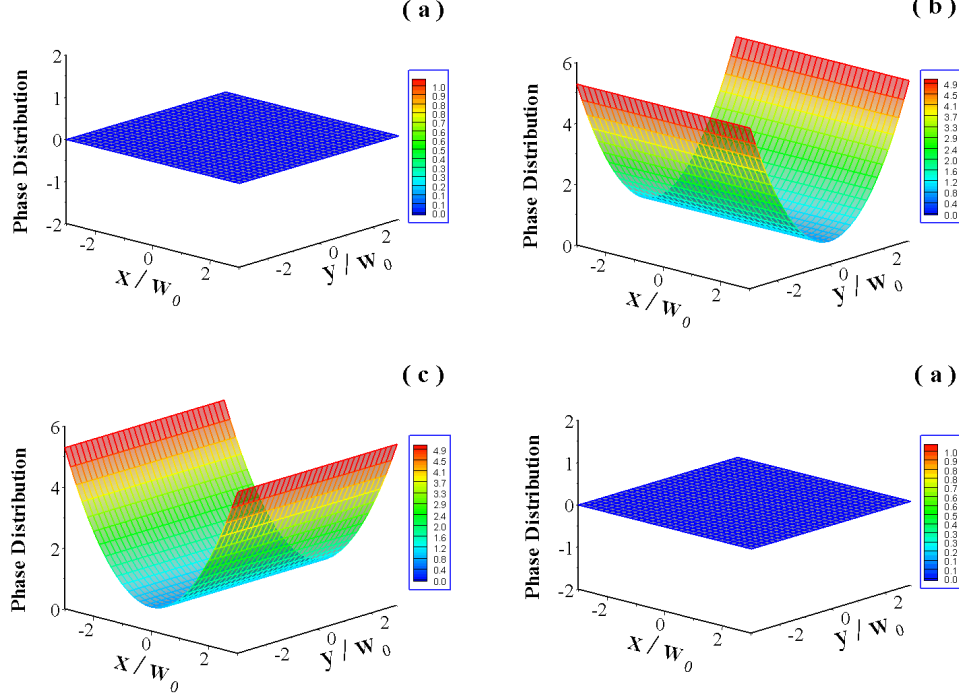


FIG. 7: The numerically computed phase distribution in object and image planes. (a) The phase distribution in object plane. The phase distribution in image plane after the Gaussian beam propagating through the QIMM slab with different anisotropic parameters: (b)  $n_x = -1$ ,  $n_y = -2$ . (c)  $n_x = -2$ ,  $n_y = -1$ . (d)  $n_x = -1$ ,  $n_y = -1$ . The phase distribution can be completely reconstructed at the image plane. The parameters are the same as in Fig. 5.

through an optical system with positive index [30, 31, 32]. While in the QIMM slab system we expect that the phase difference caused by Gouy phase shift can be compensated by that caused by the inverse Gouy shift in the QIMM slab.

We might suspect whether the phase difference caused by the Gouy phase shift in vacuum can be compensated by that caused by the inverse Gouy phase shift in QIMM slab. To obtain the better physical picture, the schematic distribution of phase fronts are plotted in Fig. 6. The phase fronts of a focused Gaussian beam are plotted with solid lines, and the phase fronts of a perfect spherical wave with the dashed lines. The phase difference on the optical axis is caused by the Gouy phase shift. The inherent secret underlying the reverse Gouy phase shift in the QIMM slab is the waves undergo a negative phase velocity.

Let us investigate what happens if we consider the phase difference caused by Gouy shift. Under the focusing matching conditions, the phase difference caused by the Gouy phase

shift in the three regions are given by

$$\begin{aligned}\Delta\Phi_1 &= -\arctan\frac{a}{z_R}, \\ \Delta\Phi_2 &= \arctan\frac{a}{z_R} + \arctan\frac{b}{z_R}, \\ \Delta\Phi_3 &= -\arctan\frac{b}{z_R}.\end{aligned}\tag{46}$$

The first and third Equations dictate the phase difference caused by the Gouy shift in regions 1 and 3, respectively. The second equation denotes the phase difference caused by the inverse Gouy phase shift in QIMM slab. Subsequent calculations of Eq. (46) show

$$\Delta\Phi_1 + \Delta\Phi_2 + \Delta\Phi_3 = 0.\tag{47}$$

This means that the phase difference caused by the Gouy phase shift in vacuum can be compensated by that caused by the inverse Gouy phase shift in QIMM slab. Therefore the condition for phase compensation can be simply written as

$$(a + b)k_0 + \sigma\sqrt{\varepsilon_y\mu_x}dk_0 = 0.\tag{48}$$

The first term in Eq. (48) are the phase deference caused by the plane wave in vacuum, and the other term is the phase deference caused by the plane wave in QIMM slab. For the purpose of illustration, the phase distribution in object plane is plotted in Fig. 7a. Generally, the phase distributions in image plane is distorted as shown in Fig. 7b and Fig. 7c. As mentioned above, the phase distortion is caused by the effect of anisotropic diffraction.

Now an interesting question naturally arises: whether the matching conditions of focusing and the phase compensation can be satisfied simultaneously. Clearly, if we seek a solution satisfying Eqs. (36) and (48), the only possibility is

$$\varepsilon_x = \varepsilon_y, \quad \varepsilon_y\mu_z = 1.\tag{49}$$

Under the matching conditions, the intensity and phase distributions at the object plane can be completely reconstructed at the image plane.

It should be mentioned that, for the QIMM slab with double-sheeted hyperboloid wave-vector surface, both E- and H-polarized beams can also exhibit the same intensity and phase reconstructed effect. Because of the positive phase velocity embedded in this type of QIMM, the paraxial beam will experience the positive Rayleigh distance and Gouy phase shift. Therefore the accumulated phase delay effect give rise to a large phase deference between the object and image planes.



## VI. DISCUSSIONS AND CONCLUSIONS

In conclusion, we have proposed how to employ the QIMM slab creat a polarization insensitive lens by the QIMM slab, in which both E- and H-polarized waves exhibit the same refocusing effect. For shallow incident angles the QIMM slab will provide some degree of refocusing in the same manner as an isotropic negative index material. We have investigated the focusing and phase compensation of paraxial beams by the QIMM slab. We have introduced the concepts of inverse Gouy phase shift and negative Rayleigh length of paraxial beams in QIMM. We have shown that the phase difference caused by the Gouy phase shift in vacuum can be compensated by that caused by the inverse Gouy phase shift in the QIMM slab. If certain matching conditions are satisfied, the intensity and phase distributions at object plane can be completely reconstructed at the image plane. In spite of potential difficulties in the road to a practical polarization insensitive lens, the essential physics described in this paper may have been observed in a different system. An extremely promising material has been previously explored in certain designs of photonic crystals, which can be effectively modelled with anisotropic permittivity and permeability tensors [33, 34, 35]. In spite of some potential technical difficulties, we wish the essential physics described in this paper will provide reference in the road to construct the polarization insensitive lens.

### Acknowledgments

This work was partially supported by projects of the National Natural Science Foundation of China(Nos. 10125521 and 10535010).

- 
- [1] V.G. Veselago, Sov. Phys. Usp. 10 (1968) 509.
  - [2] D.R. Smith, W.J. Padilla, D.C. Vier, S.C. Nemat-Nasser, S. Schultz, Phys. Rev. Lett. 84 (2000) 4184.
  - [3] R.A. Shelby, D.R. Smith, S. Schultz, Science 292 (2001) 77.
  - [4] J. Pacheco Jr., T.M. Grzegorzcyk, B.I. Wu, Y. Zhang, J.A. Kong, Phys. Rev. Lett. 89 (2002) 257401.
  - [5] C.G. Parazzoli, R.G. Greegpr, K. Li, B.E.C. Koltenba, M. Tanielian, Phys. Rev. Lett. 90 (2003) 107401.

- [6] A.A. Houck, J.B. Brock, I.L. Chuang, Phys. Rev. Lett. 90 (2003) 137401.
- [7] M. Notomi, Phys. Rev. B 62 (2000) 10696.
- [8] C. Luo, S.G. Johnson, J.D. Joannopoulos, J.B. Pendry, Phys. Rev. B 65 (2002) 201104.
- [9] C. Luo, S.G. Johnson, J.D. Joannopoulos, Appl. Phys. Lett. 81 (2002) 2352.
- [10] J. Li, L. Zhou, C.T. Chan, P. Sheng, Phys. Rev. Lett. 90 (2003) 083901.
- [11] I.V. Lindell, S.A. Tretyakov, K.I. Nikoskinen, S. Ilvonen, Microw. Opt. Technol. Lett. 31 (2001) 129.
- [12] L.B. Hu, S.T. Chui, Phys. Rev. B 66 (2002) 085108.
- [13] D.R. Smith and D. Schurig, Phys. Rev. Lett. 90 (2003) 077405.
- [14] Y. Zhang, B. Fluegel, A. Mascarenhas, Phys. Rev. Lett. 91 (2003) 157401.
- [15] H. Luo, W. Hu, X. Yi, H. Liu and J. Zhu, Opt. Commun. 254 (2005) 353.
- [16] H. Luo, W. Hu, W. Shu, F. Li and Z. Ren, Europhysics Letters, **74** (2006) 1081.
- [17] J.B. Pendry, Phys. Rev. Lett. **85**, 3966 (2000).
- [18] D.R. Smith, D. Schurig, J.J. Mock, P. Kolinko, P. Rye, Appl. Phys. Lett. **84**, 2244 (2004).
- [19] D.R. Smith, P. Kolinkp, D. Schurig, J. Opt. Soc. Am. B **21**, 1032 (2004).
- [20] C.G. Parazzoli, R.B. Gregor, J.A. Nielsen, M.A. Thompson, K. Li, A.M. Vetter, D.C. Vier Appl. Phys. Lett. **84** (2004) 3232.
- [21] T. Dumelow, J.A.P. da Costa, V.N. Freire, Phys. Rev. B **72**, 235115 (2005).
- [22] M. Born, E. Wolf, Principles of Optics, University Press, Cambridge, 1997.
- [23] N. H. Shen, Q. Wang, J. Chen, Y. X. Fan, J. Ding, H. T. Wang, Y. Tian, and N. B. Ming, Phys. Rev. B **72**, 1531041 (2005).
- [24] H. Luo, W. Shu, F. Li, and Z. Ren, Opt. Commun. In Press (2006).
- [25] J.W. Goodman, Introduction to Fourier Optics, McGraw-Hill, New York, 1996.
- [26] M. Lax, W.H. Louisell, W. McKnight, Phys. Rev. A **11**, 1365 (1975).
- [27] A. Ciattoni, B. Crosignani, and P. Di Porto, Opt. Commun. **177**, 9 (2000).
- [28] H. Luo, W. Hu, Z. Ren, W. Shu, and F. Li, Opt. Commun. In Press (2006).
- [29] S. Feng, H.G. Winful, Opt. Lett. **26**, 485 (2001).
- [30] M.F. Erden, H.M. Ozaktas, J. Opt. Soc. Am. A **14**, 2190 (1997).
- [31] S. Feng and H.G. Winful, J. Opt. Soc. Am. A **16**, 2500 (1999).
- [32] S. Feng and H.G. Winful, Phys. Rev. E **61**, 862 (2000).
- [33] G. Shvets, Phys. Rev. B **67**, 0351091 (2003).

- [34] G. Shvets and Y. A. Urzhumov, Phys. Rev. Lett. **93**, 2439021 (2004).
- [35] Y. A. Urzhumov and G. Shvets, Phys. Rev. E **72**, 0266081 (2005).